Experimental determination and sensitivity analysis of the fatigue critical distances obtained with rounded V-notched specimens

C. Santus[a,*], D. Taylor[b], M. Benedetti[c]

[a]*Department of Civil and Industrial Engineering, University of Pisa, Italy.*
[b]*Department of Mechanical & Manufacturing Engineering, Trinity College Dublin, Ireland.*
[c]*Department of Industrial Engineering, University of Trento, Italy.*

Abstract

The critical distance inverse search procedure, recently proposed by the authors (Santus et al., Int. J. Fatigue, 106 (2018) 208-218), was experimentally applied in this work on 42CrMo4+QT steel and 7075-T6 aluminium alloy under load ratios R=-1 and R=0.1. The Point Method critical distance lengths resulted higher than the Line Method values, especially for notch radius much larger than the critical distance itself, obtaining almost a factor of 2 for blunt notch which is consistent with the limit condition of zero stress curvature distribution. Comparison results were reported on an accuracy chart, showing that a small radius notched specimen is recommended to determine the critical distance and then obtain an accurate strength assessment of a blunter specimen (or component), both with the Point and the Line Methods. This critical distance determination procedure was extended to the finite life regime, obtaining accurate predictions especially for the aluminium alloy. Finally, the online version of the paper is provided with MATLAB scripts containing examples for the inverse search and the direct problem calculation.

Keywords: critical distance determination; Line Method; Point Method; rounded V-notched specimen; 42CrMo4+QT; 7075-T6.

*Corresponding author: Ciro Santus
Ph. +39 (0)50 2218007
Email address: ciro.santus@ing.unipi.it (C. Santus)

Nomenclature

TCD	Theory of Critical Distances
LM, PM	Line Method and Point Method
SIF	Stress Intensity Factor
N-SIF	Notch SIF
ΔK_{th}	Crack threshold SIF range
$\Delta\sigma_{\text{fl}}$	Plain specimen fatigue limit range
L_{th}	Critical distance obtained with the crack threshold
$\Delta\sigma_{\text{N,fl}}$	Notched specimen fatigue limit range, nominal stress
K_{f}	Fatigue stress concentration factor
D	Specimen outer diameter
R	Notch radius
A	Notch depth
ρ	Notch radius ratio
α	Notch angle
s	Williams' power law singularity exponent
$K_{\text{N,UU}}$	N-SIF for unitary nominal stress and unitary half diameter
L	Critical distance obtained with the LM
l	Dimensionless critical distance obtained with the LM
L_0	Singular term critical distance obtained with the LM
l_0	Dimensionless singular term critical distance obtained with the LM
l_{min}	Minimum limit for the range of accurate critical distance determination
l_{max}	Maximum limit for the range of accurate critical distance determination
$\gamma(l)$	Inversion function for the LM critical distance determination
γ_{min}	Minimum value of the inversion function range
γ_{max}	Maximum value of the inversion function range
β	Line slope of the LM inversion function
$p_1, \ldots, p_4$	Model function coefficients for l_{min}
$q_1, \ldots, q_4$	Model function coefficients for γ_{min}
c_1, c_2, c_3	Model function coefficients for l_{max}
L'	Critical distance obtained with the PM

l'	Dimensionless critical distance obtained with the PM
L'_0	Singular term critical distance obtained with the PM
l'_0	Dimensionless singular term critical distance obtained with the PM
$\gamma'(l')$	Inversion function for the PM critical distance determination
$\delta_1, \ldots, \delta_5$	Coefficients for the PM polynomial inversion function
S, S'	Critical distance sensitivity with respect to K_f for LM and PM respectively
R	Fatigue load ratio
σ_a	Stress amplitude
N_f	Number of cycles to failure
k, b	Constants of the Basquin's law, Eq. 10
k_1, k_2, m	Constants of a different S-N curve formulation, Eq. 11
$\sigma_{\mathrm{a},i}$	i-th fatigue amplitude data point
$\hat{\sigma}_{\mathrm{a},i}$	i-th fatigue amplitude data point estimator
σ	Statistical standard deviation of the data, Eq. 12
q	Number of data elements
p	Number of parameters in the regression
C, n	Klesnil-Lukáš law constants, Eq. 13

1. Introduction

A reliable fatigue prognosis necessitates robust notch fatigue assessment methods, as almost any machine element contains geometrical details resulting in stress concentration effects. Among various methods proposed in the past [1, 2, 3, 4] to deal with notch fatigue calculation, the Theory of Critical Distances (TCD), originally devised by Neuber [5] and Peterson [6] in the 50's of the past century, has experienced a new golden age in the last two decades [7]. The theory has been successfully applied to predict high to medium-cycle fatigue [8, 9], also in the presence of residual stresses [10, 11, 12], multiaxial and variable amplitude fatigue [13], fretting fatigue [14, 15, 16], fatigue of welded joints [17], and even static brittle fracture [18]. The basic idea is that the critical condition in a notched or cracked member is achieved when a suitable stress component evaluated at a certain critical distance or averaged over a domain of a certain critical size equals a stress value representative of the fatigue (or static) failure in a smooth part. The former approach is known as the Point Method (PM), the latter methods consider averaging domains of different dimensionality [7, 19]. Among them, the most common is the

Line Method (LM), which proved to yield more accurate estimations in comparison with methods considering averaging domains of higher geometrical complexity [3].

In the context of notch fatigue calculation, which is the subject of the present work, the Critical Distance length is defined on the base of the threshold Stress Intensity Factor (SIF) range ΔK_{th} and the plain specimen fatigue limit full range $\Delta\sigma_{\text{fl}}$:

$$L_{\text{th}} = \frac{1}{\pi}\left(\frac{\Delta K_{\text{th}}}{\Delta\sigma_{\text{fl}}}\right)^2 \tag{1}$$

The symbol L_{th} is here introduced to specify that this value is inferred from the stress intensity factor threshold, and L_{th} is then considered in the following as the reference for comparison with the lengths L and L' derived from the LM and the PM, respectively. The former is used to average the stress over $2L$, the latter to estimate the stress at the location $L'/2$ from the notch tip. In principle, the three lengths: L_{th}, L, L' should be coincident since they take exactly the same value when the crack geometry and the related singular stress term considered. Nevertheless, these three lengths are experimentally defined here in different ways, as better explained below, and comparisons and discussion are provided.

While the determination of notched specimen fatigue limit requires experimental equipment and expertise usually within reach of any material testing laboratory, an accurate measurement of the threshold may be a challenging experiment, especially at negative load ratios R. Moreover, the status of the material at the crack tip is different from the machined condition typical of geometrical details present in machine elements and, for some materials, this may cause inaccuracy in terms of strength assessment. Even though the procedure for experimental threshold determination is codified in standards, as ASTM E647 [20], there is large variability in the threshold values published in the technical literature. This is due to both inevitable fluctuations in chemical composition, texture and microstructure in nominally identical materials and the high sensitivity of the threshold to the experimental procedure. The threshold is indeed strongly influenced by extrinsic crack shielding mechanisms [21, 22], such as crack closure and bridging, whose full development depends on the previous history experienced by the crack during the precracking and force-shedding phases. Regarding the aeronautical aluminium grade 7075-T6, which is one of the two materials investigated in the present paper, Forth et al. [23] reported threshold values for load ratio R = 0.1 equal to 1.45 and 2.30 MPa$\sqrt{\text{m}}$, obtained under compression precrack + constant amplitude (CPCA) and constant R load reduction (LR), respectively. Jordon et al. [24] found ΔK_{th} values of 2.10 and 2.35 MPa$\sqrt{\text{m}}$, for CPCA and LR, respectively. Petit and Zeghloul [25] found a ΔK_{th} value of 3.77 MPa$\sqrt{\text{m}}$ under LR. ASM handbook [26] reports the scatterband of fatigue crack growth curves of 7075-T651 estimated on the base of 6 tests undertaken on 3 different material lots. It is shown that the corresponding crack growth threshold ΔK_{th} is comprised between 2.1 and 2.8 MPa$\sqrt{\text{m}}$. Considering that the high-cycle fatigue strength full range of

this alloy is on the order of 240 MPa [27], the resulting scatterband in the critical distance length is between 24 and 43 μm.

Another issue related to the threshold-based definition of the critical distance L_{th} according to Eq. (1) is that it precludes the TCD from being extended to the medium-cycle fatigue regime, because it is not straightforward to define a fracture mechanics parameter representative of the crack growth resistance in this fatigue regime. To overcome all these limitations, Susmel and Taylor [28, 29] suggested determining L by calibrating a TCD method on the base of the S-N curves generated by testing specimens with two different geometries, of which at least one contains a stress concentration feature. In this way, it is possible to estimate how L varies as a function of the number of cycles to failure. Usually, a power-law equation formally identical to the Basquin's law is adopted [8, 9].

Santus et al. [30] recently proposed the use of a sharp V-notched specimen to deduce the material critical length through an analytical procedure that just requires the knowledge of the notch fatigue stress concentration factor K_{f} and the geometry dimensions. In addition, a sensitivity analysis was undertaken to identify the level of notch sharpness (mainly controlled by the notch root radius) necessary for a well-posed determination of the critical distance. The present paper is aimed at comparisons and discussion about the critical distance determination according to the crack threshold and the proposed sharp V-notch procedure, and then evaluating the suitability of the obtained values for assessing the fatigue strength of another specimen considered as a potential component to be designed. This investigation was performed on two structural metal alloys, namely 42CrMo4+QT steel and 7075-T6 aluminium alloy, under load ratios $\text{R} = 0.1$ and $\text{R} = -1$. For this purpose, fatigue tests in the medium to high cycle regime and fatigue crack growth rate tests were carried out, providing a complete set of fatigue data which allowed several cases to be analysed and finally the extension to the fatigue finite life.

2. Critical distance determination procedure

The critical distance inverse search determination procedure proposed by Santus et al. [30] is briefly summarized in this section. The specimen dimensions are defined in Fig. 1 (a), A is the notch depth, R is the notch radius, α is the notch angle and D is the other diameter of the specimen, while in Fig. 1 (b) the main formulas are reported to obtain L and L' according to the Line and Point Methods respectively.

The LM inverse search requires a first evaluation of the critical distance length based on the stress singular term distribution:

$$l_0 = \frac{1}{2}\left(\frac{K_{\text{N,UU}}}{(1-s)\,K_{\text{f}}}\right)^{1/s} \tag{2}$$

where $K_{\text{N,UU}}$ is the dimensionless (net) Notch Stress Intensity Factor (N-SIF) for unitary nominal stress and

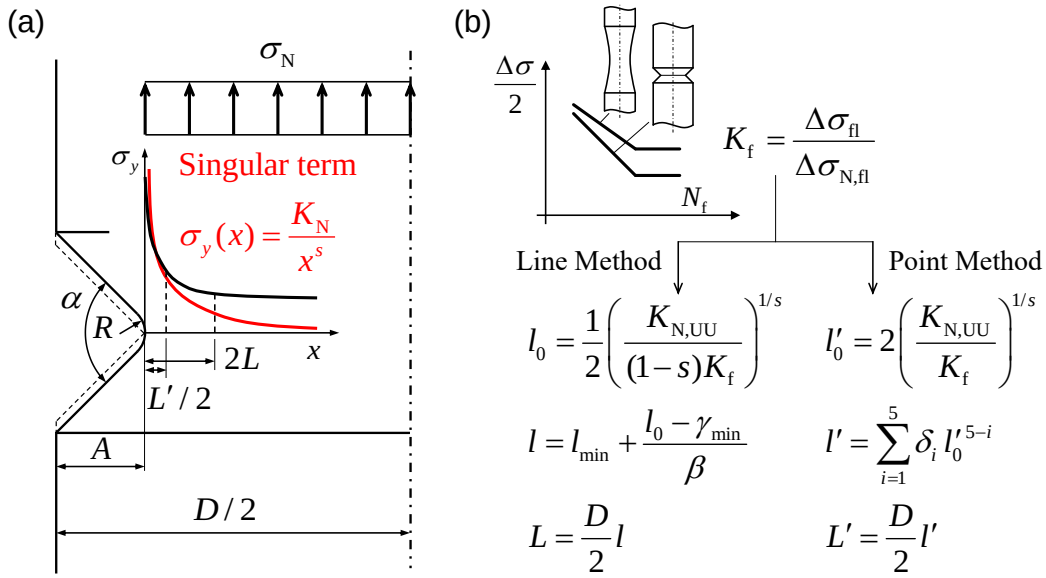

Figure 1: (a) Notched specimen dimensions. (b) Summary of the LM and PM inverse search procedures.

unitary scaling length, i.e. when the specimen radius $D/2$ equals unity, and s is Williams' power law singularity exponent. After having calculated this length, the LM dimensionless critical distance is obtained by means of the linear model:

$$l = l_{\min} + \frac{l_0 - \gamma_{\min}}{\beta} \tag{3}$$

where:

$$\beta = \frac{\gamma_{\max} - \gamma_{\min}}{l_{\max} - l_{\min}} \tag{4}$$

and these parameters can be obtained as equation models as a function of the notch radius ratio $\rho = R/A$:

$$\begin{aligned} l_{\min} &= p_1\rho^3 + p_2\rho^2 + p_3\rho + p_4 \\ \gamma_{\min} &= q_1\rho^3 + q_2\rho^2 + q_3\rho + q_4 \\ l_{\max} &= \gamma_{\max} = c_1 + c_2\rho^{c_3} \end{aligned} \tag{5}$$

$l_{\min}, l_{\max}$ are not only the coefficients for the calculation but also the limit values of an accuracy range in which the critical distance length is expected to be found, and $\gamma_{\min}, \gamma_{\max}$ are the correction function corresponding values. A similar procedure is followed for the PM. The singular term length is initially calculated:

$$l'_0 = 2\left(\frac{K_{N,UU}}{K_f}\right)^{1/s} \tag{6}$$

and the dimensionless PM critical distance is then obtained with a polynomial model:

$$l' = \delta_1 \, l_0'^4 + \delta_2 \, l_0'^3 + \delta_3 \, l_0'^2 + \delta_4 \, l'_0 + \delta_5 \tag{7}$$

where the coefficients δ_i, $i = 1,\ldots,5$ can be obtained by interpolating tabular values as functions of the notch radius ratio ρ.

The dimensional LM critical distance is finally obtained as:

$$L = (D/2)\, l \tag{8}$$

and in the same way the PM length:

$$L' = (D/2)\, l' \tag{9}$$

This modelling can be reversed if the material characteristic length L is known (or assumed to be known) and the searched quantity is the fatigue stress concentration factor K_{f} of the specimen, which can be seen as the "direct problem" since it is the natural way of the critical distance analysis. The LM direct problem can be solved straightforwardly owing to the (modelled) linearity between l_0 and l, while the PM requires a numerical procedure since Eq. 7 cannot be easily inverted. However, in the range $l_{\min} - l_{\max}$ this polynomial function is strictly monotonically increasing and then the inversion can be obtained with a numerical algorithm, as suggested in Ref. [30] where the overall procedure is explained in details.

These calculations can be easily implemented by running the MATLAB® script files, available in the online page of the paper as supplementary material, which load all the coefficients available in Ref. [30] and then provide inverse search and direct problem examples. Appendix A briefly explains these scripts and the numerical values to be obtained.

3. Materials and fatigue test results

The experimentation is performed on samples extracted from a unique supply of bars of 60 mm diameter to avoid any material mismatch due to slightly different heat treatment or material composition. Specifically, rolled bars of 42CrMo4+QT steel (Quenched and Tempered), DIN number 1.7225, very similar to American standard AISI4140, and extruded bars of aeronautical aluminium grade 7075-T6 are used.

Fig. 2 (a) and (b) illustrates the microstructure of 42CrMo4+QT, while (c) and (d) the aluminium alloy 7075-T6, on the cross-section normal and parallel to the longitudinal (L) rolling/extrusion direction of the bars, respectively. 42CrMo4+QT displays the characteristic globular microstructure (sorbite) of tempered martensite, consisting of a fine interspersion of α-ferrite and non-acicular cementite. The aluminium alloy exhibits equiaxial pancake grains (grain size comprised between 40 and 80 μm) on the plane normal to the L-direction and elongated grains (average grain thickness 10 μm) along the rolling direction. A fine interspersion of intermetallic precipitates is also visible.

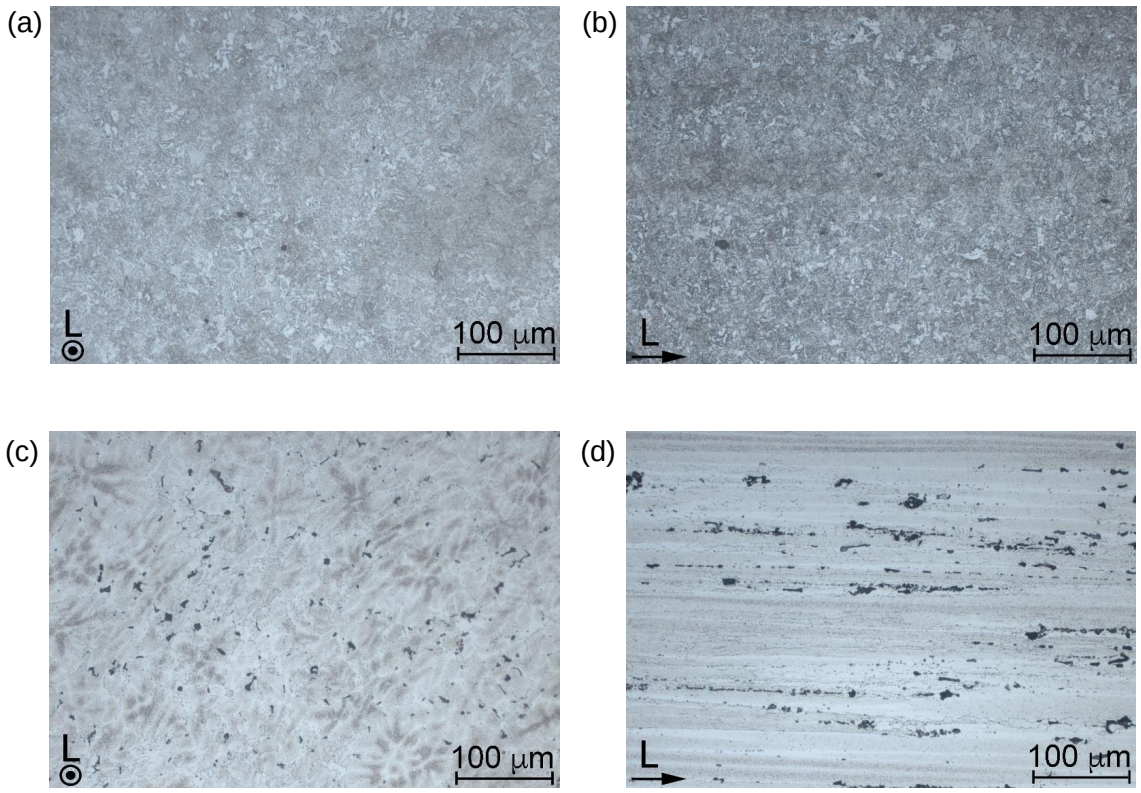

Figure 2: Optical micrographs of the investigated materials' microstructure: (a) and (b) 42CrMo4+QT steel, (c) and (d) 7075-T6 Al alloy; (a) and (c) sections taken perpendicularly to, (b) and (d) along the longitudinal (L) direction.

Monotonic tensile tests (initial strain rate of 10^{-4} s^{-1}) are performed according to the standard ASTM E8 on dog-bone specimen aligned with the longitudinal (L) orientation of the bars. Three tests are replicated for each condition, the yield strength is determined as the 0.2% offset yield stress and all the tensile test results are summarized in Table 1.

Table 1: Tensile test results of the two investigated metal alloys.

42CrMo4+QT	E, GPa	S_Y, MPa	S_U, MPa	S_f, MPa	%El	%RA
Mean	206	727	875	566	17.6	57.7
St. dev.	5.90	13.9	15.0	16.2	2.52	0.433
7075-T6	E, GPa	S_Y, MPa	S_U, MPa	S_f, MPa	%El	%RA
Mean	70.5	531	595	577	10.0	13.2
St. dev.	0.231	7.30	5.86	2.20	0.728	4.57

The fatigue characterization is carried out in the L-orientation on axisymmetric specimens, whose geometry is illustrated in Fig 3. Specifically, plain (smooth) specimens are used to determine the materials' baseline fatigue S-N curve.

Two types of V-notched samples are employed to assess the material notch sensitivity. The *sharp* specimen (Fig. 4) was obtained by machining at the notch tip whithout imposing a fillet path of the tool, in order to replicate

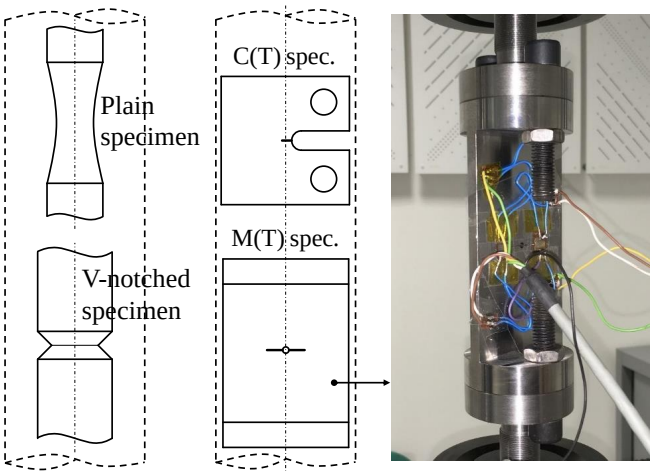

Figure 3: Different specimens extracted from the same bar supply: plain and V-notched specimens, C(T) and M(T) specimens, and picture of a M(T) specimen with attached crack length foils and flange joints.

the tool corner radius and obtain the sharpest notch with a specific tool. The insert used had a corner radius of 0.2 mm. Even smaller corner radius of 0.1 mm inserts are commercially available, however the blunting of the insert should be checked during the machining of the entire number of specimens, and then actual local radius should be verified. Whereas, the *blunt* specimen is intentionally provided with a larger notch root fillet radius of 1 mm to provide L assessment comparisons.

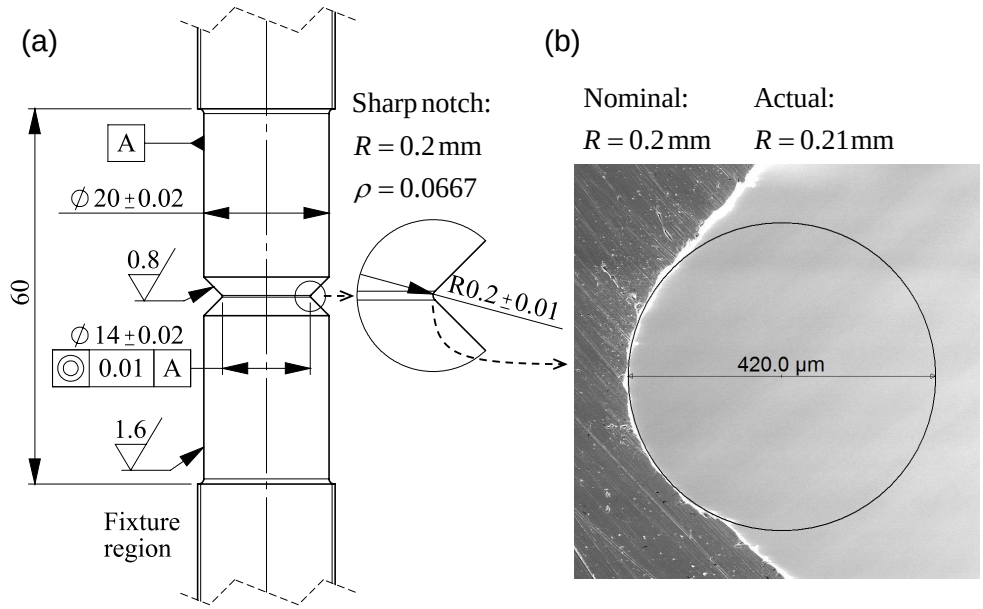

Figure 4: (a) Drawing of the sharp V-notched specimen, dimensions and recommended manufacturing tolerances. (b) Evidence of the actual notch radius after a cross section.

Alternating (zero mean stress, load ratio $R = -1$) and pulsating (load ratio $R = 0.1$) axial fatigue tests are carried out according to the standard ASTM E466 in laboratory environment using a resonant testing machine Rumul Testronic 50kN (Russenberger Prüfmaschinen, AG, Neuhausen am Rheinfall, Switzerland) operating at

a nominal frequency of 150 Hz under load control. Different strategies are pursued in fatigue testing the two materials. Some preliminary fatigue tests have been carried out on the steel coupons to explore the fatigue behaviour beyond the knee of the S-N curve with the aim of bringing the samples to failure in the very high cycle fatigue regime. Since the samples that survived 5 million cycles did not fracture even after 50 million cycles, we decided to adopt the traditional approach of assuming the existence of the fatigue limit beyond the knee of the S-N curve. The fatigue limit corresponding to a life of 10×10^6 cycles is calculated according to a staircase procedure employing $10-15$ samples and 10 MPa stress increments. The medium-to-high-cycle fatigue life in the range between nearly 5×10^4 and 10^6 cycles is explored for plain and sharp-notched samples at four load levels, using $3-4$ samples for each of them. The fatigue curves corresponding to 50% of failure probability, represented by the Basquin's model:

$$\sigma_{\mathrm{a}} = k N_{\mathrm{f}}{}^{b} \tag{10}$$

are determined by fitting the $\log(N_{\mathrm{f}})$ versus $\log(\sigma_{\mathrm{a}})$ results. The uncertainty range is assumed to be constant and approximated by its centroid value.

Conversely, the S-N curves of Al samples displayed a steadily declining trend with increasing N_{f}. Therefore, fatigue tests are carried out at different stress amplitudes to explore fatigue lives up to 30×10^6 cycles. The S-N curve for each experimental condition is obtained from 10 (blunt-notched) to 15 (plain and sharp-notched) coupons, and runout tests are terminated at 30×10^6 cycles when no fracture takes place. The S-N curves have been found to be well represented by the following model:

$$\sigma_{\mathrm{a}} = k_1 + \frac{k_2}{N_{\mathrm{f}}{}^{m}} \tag{11}$$

The scatter of the fatigue data is assessed by computing the estimated regression variance assumed to be uniform for the whole fatigue life range and expressed by:

$$\sigma^2 = \frac{\sum_{i=1}^{q} \left(\sigma_{\mathrm{a},i} - \hat{\sigma}_{\mathrm{a},i}\right)^2}{q-p} \tag{12}$$

where $\sigma_{\mathrm{a},i}$ is the i-th fatigue amplitude data point, $\hat{\sigma}_{\mathrm{a},i}$ is its estimator, q is the number of data elements, and p is the number of the parameters in the regression ($p = 3$ in the present case).

The S-N data is reported in Fig. 5 along with the fit curves, and the summary of the fatigue limits are listed in Table 2, at 10×10^6 cycles about the steel and at 30×10^6 cycles about the aluminium alloy for which a fatigue limit is assumed at this relatively high life duration.

The fatigue crack growth rate testing is performed according to the standard ASTM E647 [20]. C(T) and M(T) specimens (Fig. 3) are designed as largest width from the diameter bars of 60 mm, and they are employed to

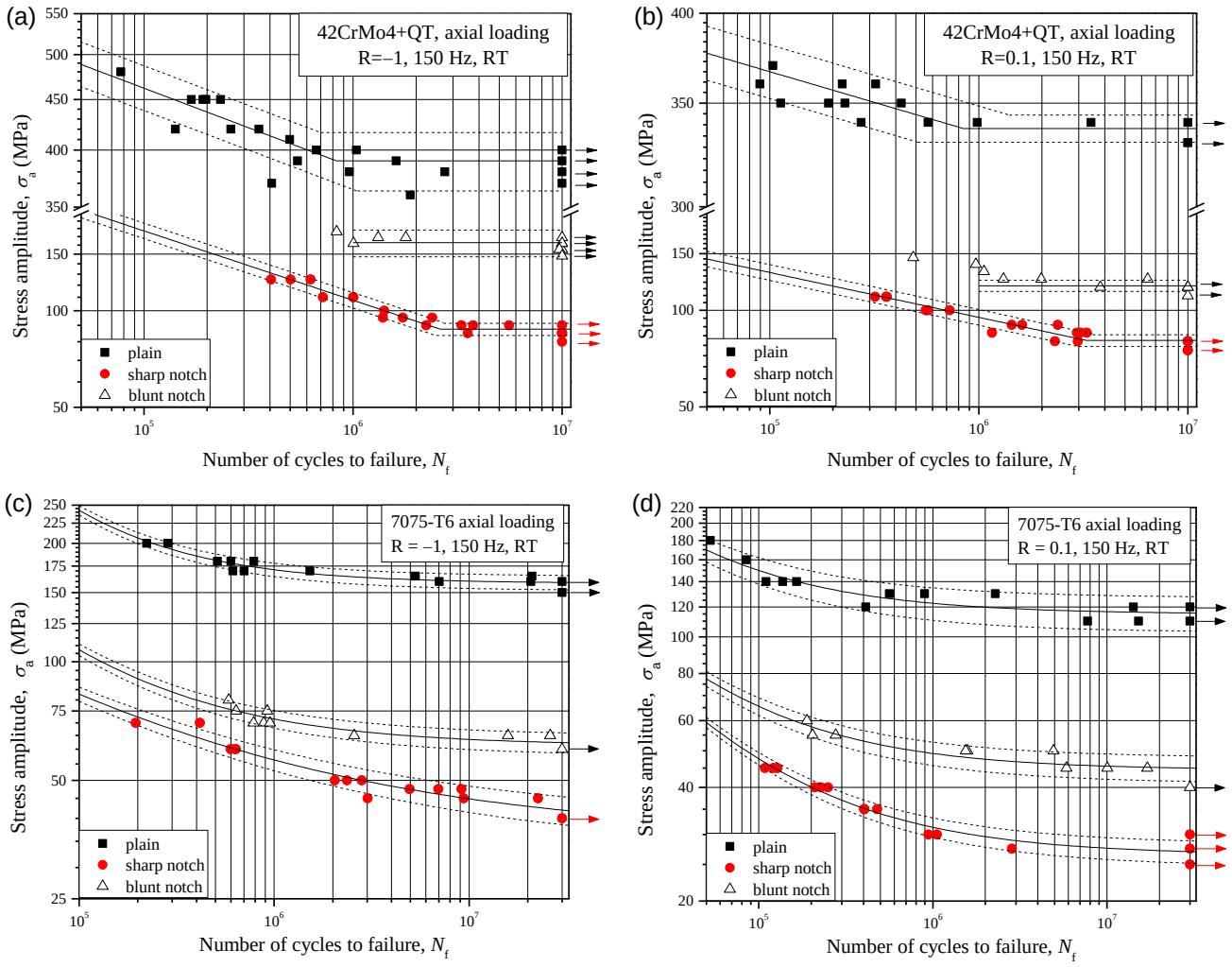

Figure 5: Plain and notched specimen fatigue experimental data and fit curves for 42CrMo4+QT (a) load ratio R $= -1$, (b) R $= 0.1$, arrows indicate runouts at 10×10^6 cycles, and 7075-T6 (c) R $= -1$, (d) R $= 0.1$, arrows indicate runouts at 30×10^6 cycles. Dashed lines correspond to the fatigue strengths for the different specimens at 10% and 90% failure probabilities.

carry out fracture mechanics tests under pulsating (R $= 0.1$) and alternating (R $= -1$) loading, respectively. They are extracted from the same supply of bars as the other specimen types so as to align the direction of the load application with the longitudinal L orientation, and have the material tested region approximately at the central axis. The crack growth takes place on the plane normal to the rolling direction. The initial notch of all specimens is Electro Discharge Machined (EDM) with a wire of 0.5 mm diameter to facilitate the follow-up pre-cracking process. The M(T) specimen is manufactured with normal lateral flanges which are bolted at two fixtures (visible in the picture of Fig. 3) to be then connected to the fatigue test machine. Two large size bolts at each side ensured closed contact during the entire load cycle, even with relatively large tensile load. The specimen width is selected in the range recommended by the ASTM standard, however quite close to the minimum value in order to limit the maximum load. Nevertheless, the buckling load of the specimen is much larger than the maximum (compressive) load required for the crack propagation, and the predominantly elastic condition is easily satisfied.

Table 2: Fatigue limits for the different specimens, load ratios and failure probability, and finite life curve parameters.

42CrMo4+QT	$R=-1$			$R=0.1$		
	Plain	Blunt	Sharp	Plain	Blunt	Sharp
$P_{50\%}$, MPa	390	163	87.5	337	119	80.5
$P_{10\%}$, MPa	363	147	83.5	330	114	77.1
$P_{90\%}$, MPa	417	178	91.3	344	124	83.9
St. dev., MPa	20.7	12.1	2.93	5.30	3.71	2.65
k, MPa	1163	n/a	2127	578.9	n/a	653.8
$b\ (\times 10^3)$	-80.139	n/a	-215.96	-39.655	n/a	-139.65
7075-T6	$R=-1$			$R=0.1$		
	Plain	Blunt	Sharp	Plain	Blunt	Sharp
$P_{50\%}$, MPa	159	62.3	42.0	116	45.0	27.0
$P_{10\%}$, MPa	152	58.7	38.5	104	41.5	25.2
$P_{90\%}$, MPa	166	66.0	45.5	128	48.5	28.9
St. dev., MPa	5.23	2.86	2.69	9.43	2.72	1.43
k_1, MPa	158.3	61.21	36.15	114.8	44.45	26.48
k_2, MPa $(\times 10^{-3})$	946.7	82.03	3.078	62.35	37.43	32.56
$m\ (\times 10^3)$	810.09	650.95	363.92	650.95	650.95	637.51

The experiments are conducted in the laboratory environment on the same resonant testing machine Rumul Testronic 50 kN. A sinusoidal pulsating load waveform is applied at a frequency of approx. 100 Hz and 160 Hz, for C(T) and M(T) specimens, respectively. A Fractomat® apparatus based on the indirect potential drop method is used to continuously measure the crack length. For this purpose, one or two crack length foils (Krak-Gage®), consisting of a conducting layer on an electrically insulating backing, are bonded on one side of the C(T) or M(T) sample and then connected to a signal conditioning module, whose output can be used to feed-back control the testing machine. Periodically, the crack length on the back face of the sample is inspected using a travelling microscope to make sure that the two crack lengths do not differ by more than 0.25 times the sample thickness, as prescribed by the ASTM standard. The crack growth rates are calculated from discrete crack length increments of 0.2 mm, necessary for reducing the microstructure induced scatter in crack growth rate. The tests are performed in two distinct phases. In the initial force-shedding phase, the applied ΔK is exponentially reduced by setting the decay constant $(1/K)(\mathrm{d}K/\mathrm{d}a) = -0.08\ \mathrm{mm}^{-1}$ until reaching near-threshold fatigue crack growth conditions. The initial ΔK is set to keep the crack growth rate below 10^{-8} m/cycle. The final part of the experiments is performed under constant force amplitude and the crack growth rate data are used to build the $\mathrm{d}a/\mathrm{d}N$ vs ΔK curves. The experimental data are represented by the exponential law, Eq. 13, proposed by Klesnil and Lukáš [31]:

$$\frac{\mathrm{d}a}{\mathrm{d}N} = C(\Delta K^n - \Delta K_{\mathrm{th}}^n) \tag{13}$$

Crack growth rate data for both materials and load ratios are reported in Fig. 6 along with the parameters of the

fit curve Eq. 13, and the corresponding threshold values have been assumed as the stress intensity range for the experimental point of each curve with the lowest propagation rate.

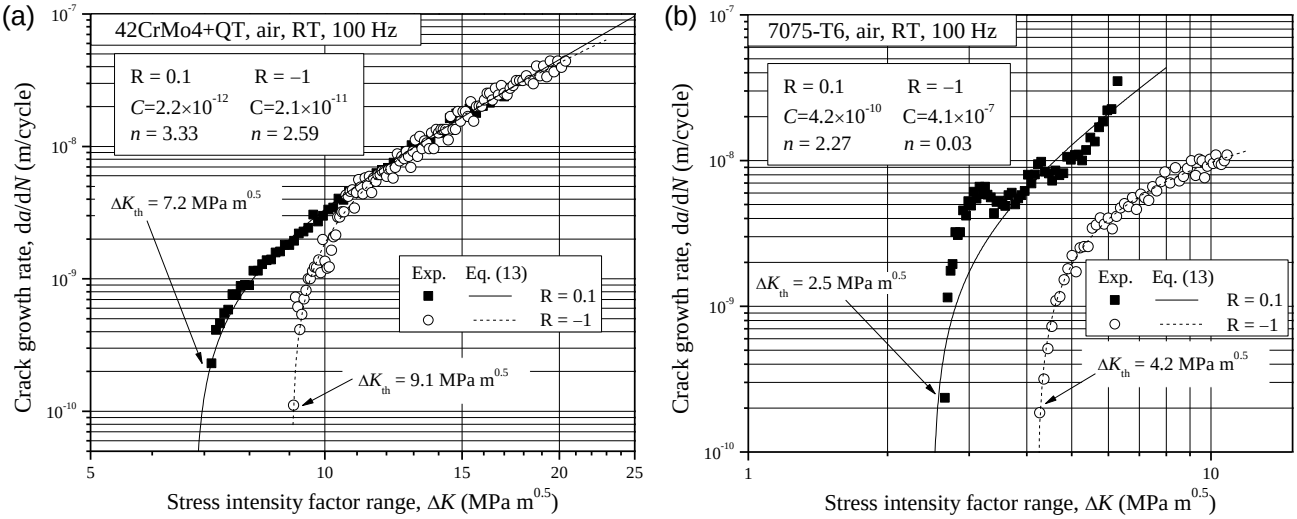

Figure 6: Crack propagation curves, threshold determination and Klesnil and Lukáš fit curve parameters for (a) 42CrMo4+QT steel and (b) 7075-T6 aluminium alloy.

The crack propagation curves of 42CrMo4+QT steel, Fig. 6 (a), indicate a remarkable effect of the load ratio R on the threshold regime, while its effect on the intermediate growth rate region is very weak. Conversely, in the Al-7075-T6 alloy, Fig. 6 (b), the load ratio effect is pronounced in all the investigated crack growth regimes. The found threshold values agree well with those reported by Noroozi et al. [32] for a similar Al alloy. Since the present paper is mainly focused on the threshold regime, we investigated the material at low crack growth rates, viz. $\mathrm{d}a/\mathrm{d}N < 10^{-8}$ m/cycle. In this regime, the slope of the crack propagation curve is unusually small while, according to Ref. [32], the curves are expected to become much steeper at higher growth rates. Moreover, the modelling proposed by Klesnil and Lukáš (Eq. 13) produced a very small n value for the aluminium alloy at $\mathrm{R} = -1$, which is not to be interpreted as the slope of the Paris's law for higher SIF ranges than in the near-threshold part of the curve.

4. Fatigue data analysis

4.1. Critical distance length determination

The availability of both the crack threshold and the notch fatigue strength, along with the plain specimen fatigue strength, allows to verify the accuracy of the inverse search critical distance estimations. As discussed by Santus et al. [30], a sensitivity parameter can be defined to evaluate the effect of any experimental bias to the inverse search critical distance determination. This parameter can be defined both about the Line and the Point

Method critical distance lengths, Eq. 14:

$$S = -\frac{1}{L}\frac{\mathrm{d}L}{\mathrm{d}K_\mathrm{f}}, \quad S' = -\frac{1}{L'}\frac{\mathrm{d}L'}{\mathrm{d}K_\mathrm{f}} \tag{14}$$

High strength metals, such as the steel and the aluminium alloy investigated here, usually feature a short critical distance on the order of few tens of microns, such as 50 μm, or even less. For this reason, by employing the blunt notched specimen (radius $R = 1.0$ mm) the sensitivity is quite high, Fig. 7, while it is optimal for the sharp notch specimen (radius $R = 0.2$ mm) whose drawing is shown in Fig. 4.

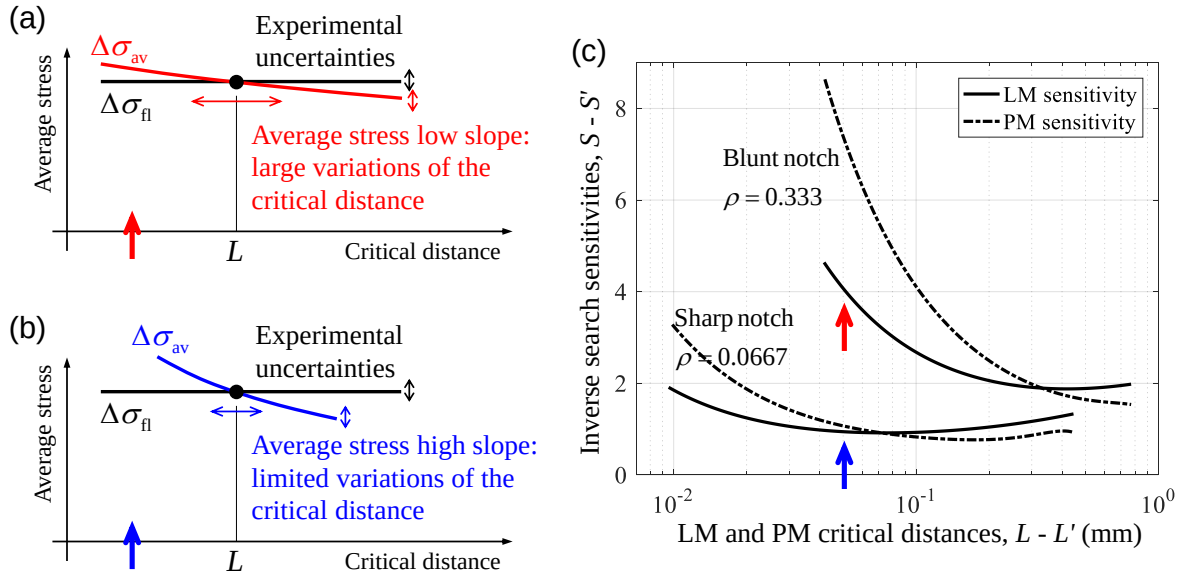

Figure 7: Inverse search sensitivity: (a) large and (b) low LM sensitivity of the deduced critical distance on the plain and the notched specimen fatigue limit variations. (c) LM and PM sensitivity functions for the sharp and the blunt notched specimens.

The comparisons between the sharp specimen LM and PM inverse search lengths with the crack threshold critical distances are shown in Fig. 8, where the inversion functions are also graphically illustrated. The notch radius $R = 0.21$ mm is introduced here as dimension input in the calculation procedure, instead of the nominal radius $R = 0.2$ mm, in agreement with Fig. 4 after specimen sectioning and observation. However, this small difference produces a quite limited effect on the deduced lengths of the order of a few percent. The LM critical distances are quite similar to the crack threshold lengths in general, while the PM values are higher. Just for the steel and load ratio $\mathrm{R} = -1$ case, the Point Method is more accurate, yet still providing a higher inverse search value than the crack threshold length. The PM inverse search critical distance is higher than the LM value because the stress curvature (second derivative) is relatively low for a rounded notch, or at least never as high as the inverse square root dependence of the crack singular term stress distribution. In principle, if the stress gradient were uniform, viz. zero stress curvature (such as in bending of a beam), the PM length would be exactly two times the LM length since the LM average stress is at $L/2$ instead of at $L/4$. The apparent convergence of the LM and PM

inverse function curves for very low L values in Fig. 8 can be misleadingly interpreted as L and L' being similar. However, for small critical distance values, the limited difference between L_0 and L_0' has a significant role and in fact L' is approximately $2L$, since the local stress is almost uniform gradient. On the other hand, when the critical distance is higher, the ratio L'/L reduces because the stress distribution curvature is relatively more significant.

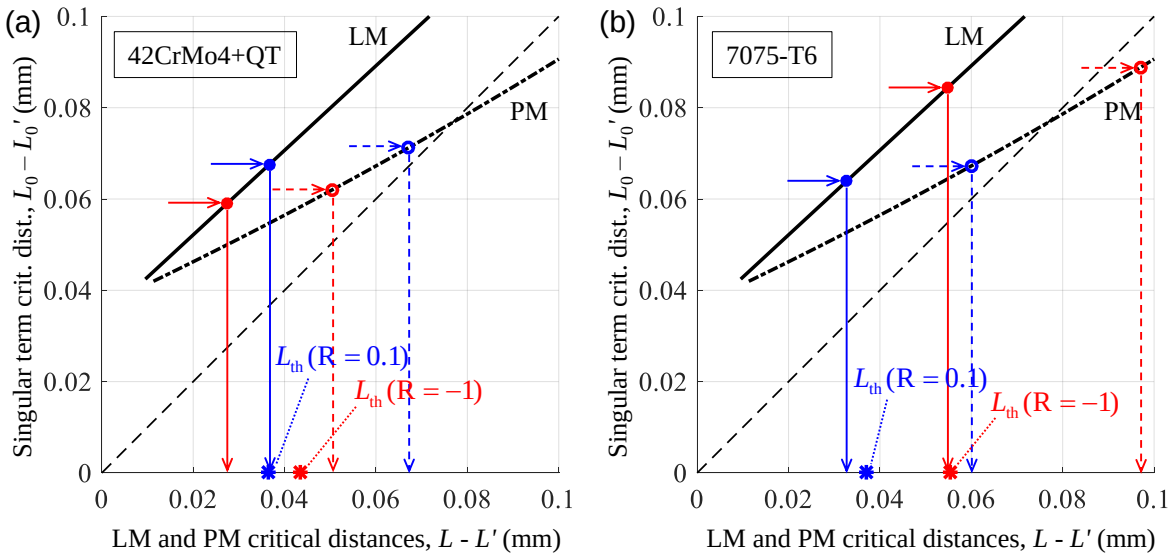

Figure 8: Sharp specimen inverse search critical distances and comparisons to the crack threshold lengths: (a) 42CrMo4+QT steel, (b) 7075-T6 aluminium alloy.

The obtained inverse search lengths are compared to the crack threshold critical distances and the percentage differences are reported in Table 3. This comparison is also provided for the *blunt* notched specimen inverse search lengths and, as expected from the sensitivity discussion, the obtained differences result much larger. Moreover for steel and R = 0.1 case, both the predicted L, L' are outside the recommended range of accuracy, in particular lower than $L_{\min}$, while this does not happen for the sharp specimen inverse search.

4.2. Strength assessments obtained with the inverse search critical distances

The critical distance length percentage difference, even for the sharp-notched specimen, can be a misleading parameter to evaluate the prediction accuracy. In fact, the critical distance in the TCD application is ultimately used to evaluate the strength of a notched component. It is worth noting that even large differences in the critical distance length do not usually produce large uncertainty in the strength prediction, unless the stress gradient is exceptionally intense, circumstance hardly ever occurring when dealing with notch radii of practical interest. In other words, the inverse search problem tends to be ill-posed and then, as a counterpart, the notch strength assessment is a well-posed problem. For this reason, it is more interesting to use the critical distance values to determine the strength of a different type of specimen and then assess, by following this way, the critical distance length prediction. Initially, the threshold SIF range can be evaluated from the notch derived lengths, just by

Table 3: Comparisons between the sharp and the blunt specimen inverse search lengths with the crack threshold critical distances.

42CrMo4+QT							
$R = -1$				$R = 0.1$			
Plain - ΔK_{th}, $L_{th} = 0.0433$ mm				Plain - ΔK_{th}, $L_{th} = 0.0363$ mm			
Plain - *Sharp*		Plain - *Blunt*		Plain - *Sharp*		Plain - *Blunt*	
LM	PM	LM	PM	LM	PM	LM	PM
L, mm	L', mm	L, mm	L', mm	L, mm	L', mm	L', mm	L', mm
0.0273	0.0505	0.0970	0.1836	0.0367	0.0671	0.0078	0.0063
-37%	17%	124%	324%	1.1%	85%	-78%	-83%
7075-T6							
$R = -1$				$R = 0.1$			
Plain - ΔK_{th}, $L_{th} = 0.0555$ mm				Plain - ΔK_{th}, $L_{th} = 0.0370$ mm			
Plain - *Sharp*		Plain - *Blunt*		Plain - *Sharp*		Plain - *Blunt*	
LM	PM	LM	PM	LM	PM	LM	PM
L, mm	L', mm	L, mm	L', mm	L, mm	L', mm	L', mm	L', mm
0.0548	0.0970	0.0589	0.1115	0.0327	0.0600	0.0535	0.1008
-1.4%	75%	6.0%	101%	-11.6%	62%	45%	173%

reversing Eq. 1. The results of this analysis are listed in Table 4, and it can be concluded the LM provides better predictions, especially for the aluminium alloy.

Table 4: Threshold SIF ranges evaluated from the inverse search critical distances.

42CrMo4+QT							
$R = -1$				$R = 0.1$			
$\Delta K_{th} = 9.1$ MPa m$^{1/2}$				$\Delta K_{th} = 7.2$ MPa m$^{1/2}$			
Plain - *Sharp*		Plain - *Blunt*		Plain - *Sharp*		Plain - *Blunt*	
LM	PM	LM	PM	LM	PM	LM	PM
7.23	9.82	13.6	18.7	7.24	9.78	3.34	3.01
-21%	8.0%	50%	106%	0.5%	36%	-54%	-58%
7075-T6							
$R = -1$				$R = 0.1$			
$\Delta K_{th} = 4.2$ MPa m$^{1/2}$				$\Delta K_{th} = 2.5$ MPa m$^{1/2}$			
Plain - *Sharp*		Plain - *Blunt*		Plain - *Sharp*		Plain - *Blunt*	
LM	PM	LM	PM	LM	PM	LM	PM
4.17	5.55	4.32	5.95	2.35	3.19	3.01	4.13
-0.7%	32%	3.0%	42%	-6.0%	27%	20%	65%

Obviously, the results in Tables 3 and 4 are closely related. By means of the inverse search lengths obtained with the sharper notched specimen, more accurate crack strength predictions are obtained. However, the percentage differences are reduced by approximately a factor of 2, when the assessment is in terms of the thresholds rather than in terms of the critical distance lengths themselves.

The fatigue strength of the notched specimen can be obtained after solving the LM and PM direct problems, as introduced above. The fatigue stress concentration factor is initially found, then the stress amplitude strength

easily calculated by multiplying by the plain specimen fatigue limit, to be finally compared to the (actual) experimental value. Initially, these evaluations have been performed with the crack threshold critical distances, and the results are reported in Table 5. The percentage errors are quite low, confirming the validity of the common usage of the TCD, in which the material length is derived from the crack threshold and then used for the fatigue assessment of notched components.

Table 5: Notched specimen fatigue predictions obtained with the crack threshold critical distances.

42CrMo4+QT							
Plain - *Crack* critical distance input							
$R=-1$, Sharp		$R=0.1$, Sharp		$R=-1$, Blunt		$R=0.1$, Blunt	
$\Delta\sigma_{N,fl}/2=87.5$ MPa		$\Delta\sigma_{N,fl}/2=80.5$ MPa		$\Delta\sigma_{N,fl}/2=163$ MPa		$\Delta\sigma_{N,fl}/2=119$ MPa	
LM	PM	LM	PM	LM	PM	LM	PM
96.9	85.0	80.3	71.3	148	143	126	123
11%	−2.8%	−0.2%	−11%	−9.0%	−12%	6.3%	3.2%
7075-T6							
Plain - *Crack* critical distance input							
$R=-1$, Sharp		$R=0.1$, Sharp		$R=-1$, Blunt		$R=0.1$, Blunt	
$\Delta\sigma_{N,fl}/2=42.0$ MPa		$\Delta\sigma_{N,fl}/2=27.0$ MPa		$\Delta\sigma_{N,fl}/2=62.3$ MPa		$\Delta\sigma_{N,fl}/2=45.0$ MPa	
LM	PM	LM	PM	LM	PM	LM	PM
42.2	36.4	27.8	24.6	61.9	59.0	43.6	42.3
0.4%	−13%	2.8%	−8.8%	−0.6%	−5.2%	−3.1%	−6.0%

More interesting is the content of Table 6 where the critical distances used for the direct problem evaluation are obtained from the inverse search, i.e. the results of Table 3. As evident from the percentage errors, quite accurate results are obtained when the critical distance is evaluated from the sharp to predict the strength of the blunt specimen, especially for the aluminium alloy. On the contrary, higher errors are observed when the length is obtained from the blunt to assess the strength of the sharp specimen. LM and PM produced approximately same results, since the different inverse search length is compensated by the consistent criterion then applied.

The results of the strength assessments reported in Tables 4, 5 and 6 can be summarized in a chart where all the three kinds of specimens are mapped, see Fig. 9. The horizontal axis of the chart represents the sort of specimen used along with the plain one to determine the critical distance length, while the vertical axis shows the accuracy in terms of prediction for the other specimen which is assessed. The errors reported in this chart are averaged as absolute values, considering both the LM and the PM result sets.

Obviously, each term of the diagonal of this chart should contain the assessment of a specimen strength with the length deduced from another specimen with the same level of sharpness. However, this was not done in the present experimental campaign, thus these errors are not available. More specifically, about the upper term of the diagonal, the critical distance should be used to predict the crack threshold of another cracked specimen, in

Table 6: Notched specimen fatigue predictions obtained with the other specimen inverse search lengths.

42CrMo4+QT							
Plain - *Blunt* critical distance input				Plain - *Sharp* critical distance input			
$R=-1$, Sharp		$R=0.1$, Sharp		$R=-1$, Blunt		$R=0.1$, Blunt	
$\Delta\sigma_{N,fl}/2=87.5$ MPa		$\Delta\sigma_{N,fl}/2=80.5$ MPa		$\Delta\sigma_{N,fl}/2=163$ MPa		$\Delta\sigma_{N,fl}/2=119$ MPa	
LM	PM	LM	PM	LM	PM	LM	PM
123	130	64.0	61.6	144	144	127	127
40%	49%	−20%	−23%	−12%	−12%	6.4%	6.4%
7075-T6							
Plain - *Blunt* critical distance input				Plain - *Sharp* critical distance input			
$R=-1$, Sharp		$R=0.1$, Sharp		$R=-1$, Blunt		$R=0.1$, Blunt	
$\Delta\sigma_{N,fl}/2=42.0$ MPa		$\Delta\sigma_{N,fl}/2=27.0$ MPa		$\Delta\sigma_{N,fl}/2=62.3$ MPa		$\Delta\sigma_{N,fl}/2=45.0$ MPa	
LM	PM	LM	PM	LM	PM	LM	PM
42.9	43.9	30.4	31.0	61.8	61.5	43.2	43.3
2.0%	4.5%	13%	15%	−0.8%	−1.3%	−4.0%	−3.8%

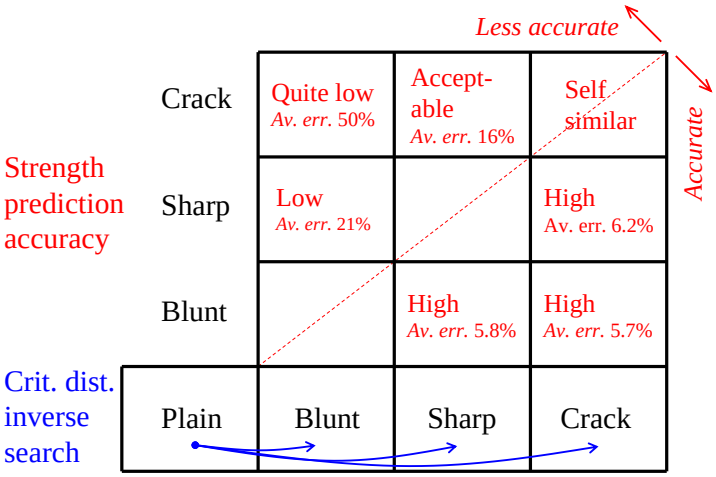

Figure 9: Different notched specimens for the critical distance determination and related fatigue strength accuracy chart.

other words by applying and then reversing Eq. 1, eventually finding the same ΔK_{th}. This case is not of interest because the TCD is circumvented, being two different (long) cracks just compared in terms of the threshold SIF range. On the other hand, the out-of-diagonal terms provide very interesting information. When the critical distance length is assessed with a sharp notch, or even the crack which can be seen as the highest level of notch sharpness, the strength prediction is very accurate (average percentage errors on the order of 6%). Whilst, if the critical distance is deduced from a specimen that is blunter than the one to be assessed, the average errors are higher, and the worst situation is to use the blunt specimen to assess the crack threshold. This principle can be stated in a more generalised way. When the strength of a notched component must be predicted and the crack threshold is not available, to obtain fatigue strength accuracy it is recommended to deduce the critical distance with a sharp, or at least sharper specimen (whenever is possible), such as the V-notched specimen proposed in this research with a proper small radius.

4.3. Scatter effect on the critical distance determination

Any fatigue strength property is affected by a certain level of scatter, such as the fatigue limits of the plain and the sharp specimens for the proposed procedure, and this in turn implies an uncertainty of the inverse search critical distance to be determined. The probabilities of failure at 90% and at 10% are taken into account here (Tab. 2) to investigate the sensitivity to a quite large scatter range. The sharp specimen fatigue stress concentration factor is calculated combining the 10% failure probability of the sharp with the 90% probability of the plain specimen and then vice-versa. The inverse search critical distances are obtained and initially compared to the 50% probability reference case. The blunt specimen strengths are then evaluated and again compared with the 50% failure probability experimental values. All these results, and the related percentage differences, are reported in Table 7. Since $\text{Plain}(P_{10\%})/\text{Sharp}(P_{90\%}) < \text{Plain}(P_{50\%})/\text{Sharp}(P_{50\%}) < \text{Plain}(P_{90\%})/\text{Sharp}(P_{10\%})$, and the lower the fatigue stress concentration factor the larger the critical distance, the lengths deduced from $\text{Plain}(P_{10\%})$ and $\text{Sharp}(P_{90\%})$ are larger than the lengths at both specimens at 50%, which again are larger than $\text{Plain}(P_{90\%})$ and $\text{Sharp}(P_{10\%})$ lengths. The ratio between the lengths of these two extreme cases is on the order of a factor of 3. However, as already found and discussed, this quite large discrepancy in terms of lengths reduces when the blunt specimen strength is evaluated. Moreover, the value of the plain specimen fatigue limit, either at 10% or 90% failure probability, contributes to mitigate the blunt specimen strength assessment uncertainty range, which in the end remains on the order of 10% for the steel and even lower for the aluminium alloy, see Table 7.

4.4. Critical distance inverse search in the finite life regime

The critical distance is usually referred to the fatigue limit (or endurance limit), or at least to a very high cycle fatigue strength for nonferrous metallic alloys. Indeed, the L_{th} value is obtained from Eq. 1 in which the threshold is involved which in turn is an "infinite-life" concept. Nevertheless, the critical distance methods, such as the Line and the Point Methods, can be extrapolated and used in the finite life regime, where the reference to a threshold stress intensity factor is lost, and then appropriate length is to be deduced as an inverse search as proposed in this research. The S-N data from Fig. 5 is reconsidered here for the entire range of the high cycle fatigue, combining the sharp and the plain specimen strengths for different numbers of cycles to failure and obtaining four critical distance curves, each material, for the two methods and the load ratios, Fig. 10. The little computational effort, required for the inverse search, permits an almost continuous length evaluation, providing high resolution curves. As the fatigue stress concentration factor reduces, for lower number of cycles to failure, the critical distance increases, even by a factor of 5 for the steel while somewhat lower for the aluminium alloy. Susmel and Taylor [8] proposed a Basquin type power law for the critical distance dependence in the finite life

Table 7: Inverse search critical distance and strength prediction sensitivity to different combinations of failure probability fatigue limits.

42CrMo4+QT							
$K_f = \text{Plain}(P_{10\%})/\text{Sharp}(P_{90\%})$				$K_f = \text{Plain}(P_{90\%})/\text{Sharp}(P_{10\%})$			
R $= -1$		R $= 0.1$		R $= -1$		R $= 0.1$	
LM	PM	LM	PM	LM	PM	LM	PM
L, mm	L', mm	L, mm	L', mm	L, mm	L', mm	L', mm	L', mm
0.0455	0.0819	0.0474	0.0851	0.0135	0.0247	0.0272	0.0502
66%	62%	29%	27%	−51%	−51%	−26%	−25%
R $= -1$, Blunt		R $= 0.1$, Blunt		R $= -1$, Blunt		R $= 0.1$, Blunt	
$\Delta\sigma_{N,fl}/2 = 163$ MPa		$\Delta\sigma_{N,fl}/2 = 119$ MPa		$\Delta\sigma_{N,fl}/2 = 163$ MPa		$\Delta\sigma_{N,fl}/2 = 119$ MPa	
139	138	127	126	149	150	127	127
−15%	−15%	6.4%	6.0%	−8.5%	−7.9%	6.5%	6.8%
$K_f = \text{Plain}(P_{10\%})/\text{Sharp}(P_{10\%})$				$K_f = \text{Plain}(P_{90\%})/\text{Sharp}(P_{90\%})$			
R $= -1$		R $= 0.1$		R $= -1$		R $= 0.1$	
LM	PM	LM	PM	LM	PM	LM	PM
L, mm	L', mm	L, mm	L', mm	L, mm	L', mm	L', mm	L', mm
0.0313	0.0575	0.0332	0.0610	0.0240	0.0444	0.0401	0.0729
14%	14%	−9.4%	−9.0%	−12%	−12%	9.3%	8.7%
R $= -1$, Blunt		R $= 0.1$, Blunt		R $= -1$, Blunt		R $= 0.1$, Blunt	
$\Delta\sigma_{N,fl}/2 = 147$ MPa		$\Delta\sigma_{N,fl}/2 = 114$ MPa		$\Delta\sigma_{N,fl}/2 = 178$ MPa		$\Delta\sigma_{N,fl}/2 = 124$ MPa	
135	135	123	123	153	153	130	130
−8.3%	−8.1%	8.0%	8.1%	−14%	−14%	4.9%	4.8%
7075-T6							
$K_f = \text{Plain}(P_{10\%})/\text{Sharp}(P_{90\%})$				$K_f = \text{Plain}(P_{90\%})/\text{Sharp}(P_{10\%})$			
R $= -1$		R $= 0.1$		R $= -1$		R $= 0.1$	
LM	PM	LM	PM	LM	PM	LM	PM
L, mm	L', mm	L, mm	L', mm	L, mm	L', mm	L', mm	L', mm
0.0835	0.1403	0.0655	0.1137	0.0321	0.0591	0.0115	0.0206
53%	45%	100%	89%	−41%	−39%	−65%	−66%
R $= -1$, Blunt		R $= 0.1$, Blunt		R $= -1$, Blunt		R $= 0.1$, Blunt	
$\Delta\sigma_{N,fl}/2 = 62.3$ MPa		$\Delta\sigma_{N,fl}/2 = 45.0$ MPa		$\Delta\sigma_{N,fl}/2 = 62.3$ MPa		$\Delta\sigma_{N,fl}/2 = 45.0$ MPa	
62.2	61.1	41.2	40.8	61.8	61.9	45.6	45.9
−0.2%	−1.8%	−8.4%	−9.3%	−0.8%	−0.7%	1.3%	2.0%
$K_f = \text{Plain}(P_{10\%})/\text{Sharp}(P_{10\%})$				$K_f = \text{Plain}(P_{90\%})/\text{Sharp}(P_{90\%})$			
R $= -1$		R $= 0.1$		R $= -1$		R $= 0.1$	
LM	PM	LM	PM	LM	PM	LM	PM
L, mm	L', mm	L, mm	L', mm	L, mm	L', mm	L', mm	L', mm
0.0467	0.0840	0.0390	0.0711	0.0624	0.1091	0.0282	0.0521
−15%	−13%	19%	18%	14%	12%	−14%	−13%
R $= -1$, Blunt		R $= 0.1$, Blunt		R $= -1$, Blunt		R $= 0.1$, Blunt	
$\Delta\sigma_{N,fl}/2 = 58.7$ MPa		$\Delta\sigma_{N,fl}/2 = 41.5$ MPa		$\Delta\sigma_{N,fl}/2 = 66.0$ MPa		$\Delta\sigma_{N,fl}/2 = 48.5$ MPa	
58.2	58.0	39.2	39.2	65.5	64.9	47.3	47.4
−0.8%	−1.1%	−5.4%	−5.5%	−0.8%	−1.7%	−2.6%	−2.3%

regime, viz. a straight line in a log-log plot, while this assumption was not perfectly verified with the results shown in Fig. 10. Though the behaviour is not very different than a straight line, the actual shape of the curve depends on the modelling of the plain and the sharp specimen S-N fit curves and ultimately on the $K_f(N_f)$ function.

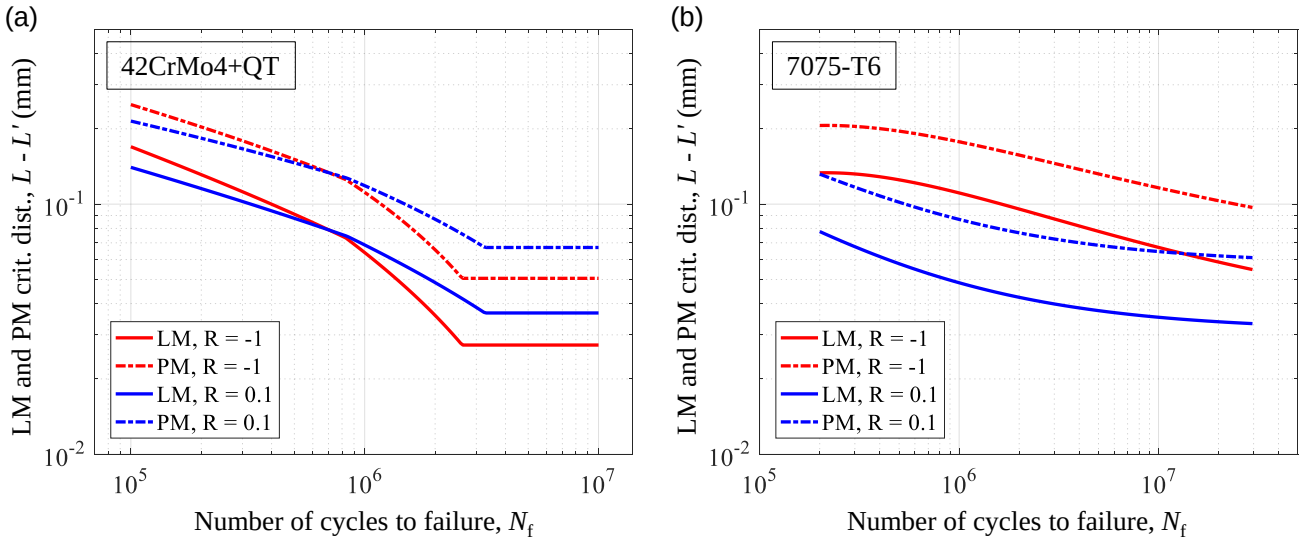

Figure 10: Critical distance inverse search in the finite life regime: (a) 42CrMo4+QT steel, (b) 7075-T6 aluminium alloy.

The steel 42CrMo4+QT curve, Fig. 10 (a), shows an intermediate knee because the plain specimen had a fatigue limit behaviour approximately at 10^6, while the sharp at a larger number of cycles. Whereas, the aluminium alloy 7075-T6 curves were modelled as single functions, hence no slope discontinuities were obtained. The load ratio $R = -1$ curves showed a zero slope tendency at 2×10^5 which is not evident for the other load ratio. Therefore, each curve can have its own peculiar behaviour, which can be properly reproduced with the present inverse search procedure, based on a point-by-point calculation and no curve shape assumption.

Similarly to the previous analysis, the calculated lengths are then used for the strength evaluation of the blunt specimen, by implementing the direct problem for each of the N_f values the finite life critical distances were derived at. Unfortunately, a limited amount of blunt specimens where available so that most of them were used to explore near the fatigue limit. For this reason, the fit curve was just horizontal for the investigated steel, while for the aluminium alloy the slope of the blunt specimens was found to be well represented by that of the plain under the load ratio $R = 0.1$, see Table 2. The blunt specimen predictions for the two metals are shown in Fig. 11. The prediction of the aluminium alloy is evidently quite accurate both as stress level and curve trend, while some inaccuracy resulted for the steel.

The different accuracy in fatigue strength estimation between the two materials can be, at least partly, explained by the onset of cyclic plasticity at the notch tip. Given the low fatigue strength and relatively high cyclic yield stress of Al alloy (see for instance the results of strain controlled LCF tests reported by Marini et al. [33] and Benedetti et al. [34]), the stress field remains in the elastic regime, hence in the limits of validity of the TCD. On the contrary, experimental investigations on 42CrMo4+QT and FE analyses of the notched specimens, not shown here for the sake of brevity, indicate that plastic deformation at the notch tip, even at stress levels close to

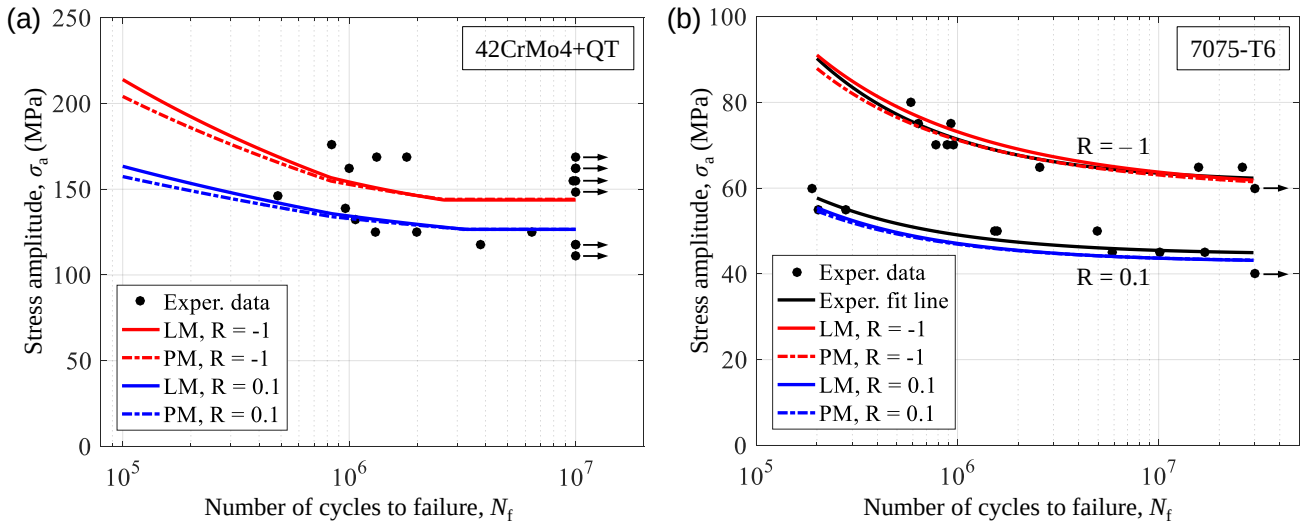

Figure 11: Finite life predictions of the blunt specimen and comparisons with the experimental data: (a) 42CrMo4+QT, (b) 7075-T6.

the fatigue limit, causes the stress field to deviate from the linear-elastic stress distribution, especially at the load ratio R $= -1$.

5. Conclusions

The critical distance inverse search procedure, as suggested by Santus et al. [30], is experimentally implemented in this work where two structural metal alloys at different load ratios are compared. This work can be regarded as a standard approach to the fatigue critical distance evaluation, without the experimental measure of the threshold stress intensity factor. Useful guidelines for the specimen geometry definition are proposed, in particular about the notch root radius, which plays an important role for a robust critical distance assessment and hence must be known and controlled with accuracy.

The Line Method and the Point Method results are compared and discussed. The PM lengths resulted higher than the corresponding LM values, especially when the critical distance length is small as compared to the notch radius, which is indeed a condition not recommended but possible. In this situation, being the stress distribution curvature relatively low, almost a factor of 2 between the PM and the LM inverse search lengths can result, while this factor reduces with a smaller radius or, equivalently, when the length to be derived is larger. The LM turned out to be more accurate, on average, in predicting the threshold critical distance lengths, especially for the aluminium alloy. Nevertheless, the PM is usually considered in critical plane multiaxial fatigue regime, thus the use of the LM could be a natural and interesting extension even for the non-proportional multiaxial fatigue.

As evident from the analysis of the experimental data, a small value to be recommended for the notch radius is 0.2 mm which is the usual turning tool corner radius. Other dimensions are obviously acceptable, however, this research suggested that the notch radius should be at least sharper than the component notch detail for which the

fatigue strength must be predicted.

This calculation has been finally extended to the fatigue finite life regime. In particular, the fast calculation of the inverse search procedure, permitted a fine sampling of evaluation points along the number of cycles to failure coordinate, thus producing a quite continuous curve and not affected by any shape assumption. Again, even in the finite life regime, it was found that the prediction is quite accurate when the sharper specimen is used for the length determination, to evaluate the fatigue strength of a blunter specimen or component.

Acknowledgments

This work was supported by the University of Pisa under the "PRA - Progetti di Ricerca di Ateneo" (Institutional Research Grants) - Project No. PRA_2016_36.

References

[1] B. Hanel, E. Haiback, T. Seeger, G. Wirthgen, H. Zenner, Analytical strength assessment of components in mechanical engineering, Forschungskuratorium Maschinenbau (FKM) Frankfurt, VDMA Verlag, 2003.

[2] B. Atzori, G. Meneghetti, L. Susmel, Material fatigue properties for assessing mechanical components weakened by notches and defects, Fatigue and Fracture of Engineering Materials and Structures 28 (1-2) (2005) 83–97. doi:10.1111/j.1460-2695.2004.00862.x.

[3] S. Götz, F. Ellmer, K.-G. Eulitz, A fracture mechanics-based approach to estimating the endurance limit of notched components, Engineering Fracture Mechanics 151 (2016) 37–50. doi:10.1016/j.engfracmech.2015.11.009.

[4] P. Lazzarin, R. Zambardi, A finite-volume-energy based approach to predict the static and fatigue behavior of components with sharp V-shaped notches, International Journal of Fracture 112 (3) (2001) 275–298. doi:10.1023/A:1013595930617.

[5] H. Neuber, Theory of notch stresses: principles for exact calculation of strength with reference to structural form and material, 2nd Edition, USAEC Office of Technical Information, 1961.

[6] R. Peterson, Notch sensitivity, in: G. Sines, J. Waisman (Eds.), Metal fatigue, McGraw Hill: New York, 1959, pp. 293–306.

[7] D. Taylor, The Theory of Critical Distances: A New Perspective in Fracture Mechanics, Elsevier Science, 2007, ISBN: 9780080444789.

[8] L. Susmel, D. Taylor, A novel formulation of the theory of critical distances to estimate lifetime of notched components in the medium-cycle fatigue regime, Fatigue and Fracture of Engineering Materials and Structures 30 (7) (2007) 567–581. doi:10.1111/j.1460-2695.2007.01122.x.

[9] R. Negru, D. Şerban, L. Marşavina, A. Magda, Lifetime prediction in medium-cycle fatigue regime of notched specimens, Theoretical and Applied Fracture Mechanics 84 (2016) 140–148. doi:10.1016/j.tafmec.2016.03.006.

[10] M. Benedetti, V. Fontanari, C. Santus, M. Bandini, Notch fatigue behaviour of shot peened high-strength aluminium alloys: Experiments and predictions using a critical distance method, International Journal of Fatigue 32 (10) (2010) 1600–1611. doi:10.1016/j.ijfatigue.2010.02.012.

[11] S. Bagherifard, C. Colombo, M. Guagliano, Application of different fatigue strength criteria to shot peened notched components. Part 1: Fracture Mechanics based approaches, Applied Surface Science 289 (2014) 180–187. doi:10.1016/j.apsusc.2013.10.131.

[12] M. Benedetti, V. Fontanari, M. Allahkarami, J. Hanan, M. Bandini, On the combination of the critical distance theory with a multiaxial fatigue criterion for predicting the fatigue strength of notched and plain shot-peened parts, International Journal of Fatigue 93 (2016) 133–147. doi:10.1016/j.ijfatigue.2016.08.015.

[13] L. Susmel, D. Taylor, A critical distance/plane method to estimate finite life of notched components under variable amplitude uniaxial/multiaxial fatigue loading, International Journal of Fatigue 38 (2012) 7–24. doi:10.1016/j.ijfatigue.2011.11.015.

[14] J. Araújo, L. Susmel, D. Taylor, J. Ferro, E. Mamiya, On the use of the Theory of Critical Distances and the Modified Wöhler Curve Method to estimate fretting fatigue strength of cylindrical contacts, International Journal of Fatigue 29 (1) (2007) 95–107. doi:10.1016/j.ijfatigue.2006.02.041.

[15] L. Bertini, C. Santus, Fretting fatigue tests on shrink-fit specimens and investigations into the strength enhancement induced by deep rolling, International Journal of Fatigue 81 (2015) 179–190. doi:10.1016/j.ijfatigue.2015.08.007.

[16] S. Vantadori, G. Fortese, C. Ronchei, D. Scorza, A stress gradient approach for fretting fatigue assessment of metallic structural components, International Journal of Fatigue 101 (2017) 1–8. doi:10.1016/j.ijfatigue.2017.04.004.

[17] L. Susmel, Modified Wöhler curve method, theory of critical distances and Eurocode 3: A novel engineering procedure to predict the lifetime of steel welded joints subjected to both uniaxial and multiaxial fatigue loading, International Journal of Fatigue 30 (5) (2008) 888–907. doi:10.1016/j.ijfatigue.2007.06.005.

[18] L. Susmel, D. Taylor, The theory of critical distances to predict static strength of notched brittle components subjected to mixed-mode loading, Engineering Fracture Mechanics 75 (3-4) (2008) 534–550. doi:10.1016/j.engfracmech.2007.03.035.

[19] D. Bellett, D. Taylor, S. Marco, E. Mazzeo, J. Guillois, T. Pircher, The fatigue behaviour of three-dimensional stress concentrations, International Journal of Fatigue 27 (3) (2005) 207–221. doi:10.1016/j.ijfatigue.2004.07.006.
[20] Standard Test Method for Measurement of Fatigue Crack Growth Rates, ASTM E647 – 15 (2015). doi:10.1520/E0647-15.
[21] R. Ritchie, Mechanisms of fatigue-crack propagation in ductile and brittle solids, International Journal of Fracture 100 (1) (1999) 55–83.
[22] M. Benedetti, E. Torresani, V. Fontanari, D. Lusuardi, Fatigue and fracture resistance of Heavy-Section ferritic ductile cast Iron, Metals 7 (3) (2017) 88. doi:10.3390/met7030088.
[23] S. Forth, J. Newman, R. Forman, On generating fatigue crack growth thresholds, International Journal of Fatigue 25 (1) (2003) 9–15.
[24] J. Jordon, J. Newman, Y. Xue, M. Horstemeyer, Near threshold fatigue crack growth in 7075-T651 aluminum alloys, in: Proceedings of the 2006 SEM Annual Conference & Exposition on Experimental & Applied Mechanics: June 4-7, 2006, Saint Louis, Missouri, USA, 2006, ISBN 091205395X.
[25] J. Petit, A. Zeghloul, On the effect of environment on short crack growth behaviour and threshold, in: K. Miller, E. de los Rios (Eds.), The Behaviour of Short Fatigue Cracks, EGF Pub. 1, Mechanical Engineering Publications: London, 1986, pp. 163–177.
[26] ASM Handbook, Fatigue and Fracture, Vol. 19, ASM International, 1996, ISBN: 0871703858.
[27] T. Zhao, Y. Jiang, Fatigue of 7075-T651 aluminum alloy, International Journal of Fatigue 30 (5) (2008) 834–849. doi:10.1016/j.ijfatigue.2007.07.005.
[28] D. Taylor, Applications of the theory of critical distances in failure analysis, Engineering Failure Analysis 18 (2) (2011) 543–549. doi:10.1016/j.engfailanal.2010.07.002.
[29] L. Susmel, D. Taylor, The Theory of Critical Distances as an alternative experimental strategy for the determination of KIc and ΔKth, Engineering Fracture Mechanics 77 (9) (2010) 1492–1501. doi:10.1016/j.engfracmech.2010.04.016.
[30] C. Santus, D. Taylor, M. Benedetti, Determination of the fatigue critical distance according to the Line and the Point Methods with rounded V-notched specimen, International Journal of Fatigue 106 (2018) 208–218. doi:10.1016/j.ijfatigue.2017.10.002.
[31] M. Klesnil, P. Lukáš, Influence of strength and stress history on growth and stabilisation of fatigue cracks, Engineering Fracture Mechanics 4 (1) (1972) 77–92. doi:10.1016/0013-7944(72)90078-1.
[32] A. Noroozi, G. Glinka, S. Lambert, Prediction of fatigue crack growth under constant amplitude loading and a single overload based on elasto-plastic crack tip stresses and strains, Engineering Fracture Mechanics 75 (2) (2008) 188–206. doi:10.1016/j.engfracmech.2007.03.024.
[33] M. Marini, V. Fontanari, M. Bandini, M. Benedetti, Surface layer modifications of micro-shot-peened Al-7075-T651: Experiments and stochastic numerical simulations, Surface and Coatings Technology 321 (2017) 265–278. doi:10.1016/j.surfcoat.2017.04.054.
[34] M. Benedetti, V. Fontanari, B. Monelli, Numerical simulation of residual stress relaxation in shot peened high-strength aluminum alloys under reverse bending fatigue, Journal of Engineering Materials and Technology, Transactions of the ASME 132 (1) (2010) 0110121–0110129. doi:10.1115/1.3184083.

Appendix A. MATLAB implementation of the inverse search procedure

MATLAB® files to automatically perform the calculations described in this research, are available in the online page of this paper as supplementary material.

Initially, it is required to run the script: `Coeffients_RunFirst.m` in order to load all the numerical coefficients required for the procedure, for both α notch angle values 90° and 60°.

An example of inverse search can be obtained by running the script `InverseSearchExample.m` with input $\alpha = 90^\circ$, specimen outer diameter $D = 20$ mm, notch depth $A = 0.3\,D/2 = 3$ mm, notch radius $R = 0.2$ mm, see Fig. 4 (a), and a tentative fatigue stress concentration factor $K_\mathrm{f} = 3.5$. The lengths obtained are: $L = 0.0734$ mm and $L' = 0.1247$ mm, along with an inverse search graph similar to Fig. 8.

Finally, an example of direct problem calculation is obtained by running the script `DirectPbExample.m`, which invokes the function `F_PMdirect.m` for the Point Method calculation and, for a verification, the previous length output values L, L' are used to back-calculate the fatigue stress concentration factor $K_\mathrm{f} = 3.5$, indeed obtaining the exact value for the LM and and quite accurate approximation for the PM.

Obviously, these example script files can be freely manipulated in several ways, for example to implement a loop calculation, instead of a single case, and find the inverse search lengths in the finite life regime for a series of K_{f} values, corresponding to an array of number of cycles to failure.